

HIGH-REDSHIFT QUASARS FOUND IN SLOAN DIGITAL SKY SURVEY
COMMISSIONING DATA¹

XIAOHUI FAN², MICHAEL A. STRAUSS², DONALD P. SCHNEIDER³, JAMES E. GUNN²,
ROBERT H. LUPTON², BRIAN YANNY⁴, SCOTT F. ANDERSON⁵, JOHN E. ANDERSON,
JR.⁴, JAMES ANNIS⁴, NETA A. BAHCALL², J. A. BAKKEN⁴, STEVEN BASTIAN⁴, EILEEN
BERMAN⁴, WILLIAM N. BOROSKI⁴, CHARLIE BRIEGEL⁴, JOHN W. BRIGGS⁶, J.
BRINKMANN⁷, MICHAEL A. CARR², PATRICK L. COLESTOCK⁴, A. J. CONNOLLY⁸, J. H.
CROCKER⁹, ISTVÁN CSABAI^{9,10}, PAUL C. CZARAPATA⁴, JOHN ERIC DAVIS⁷, MAMORU
DOI¹¹, BRIAN R. ELMS^{2,12}, MICHAEL L. EVANS⁵, GLENN R. FEDERWITZ⁴, JOSHUA A.
FRIEMAN^{4,13}, MASATAKA FUKUGITA^{14,15}, VIJAY K. GURBANI^{4,16}, FREDERICK H.
HARRIS¹⁷, TIMOTHY M. HECKMAN⁹, G. S. HENNESSY¹⁸, ROBERT B. HINDSLEY¹⁸,
DONALD J. HOLMGREN⁴, CHARLES HULL¹⁹, SHIN-ICHI ICHIKAWA¹², TAKASHI
ICHIKAWA²⁰, ŽELJKO IVEZIĆ², STEPHEN KENT⁴, G. R. KNAPP², RICHARD G. KRON^{13,4},
D.Q. LAMB¹³, R. FRENCH LEGER⁵, SIRILUK LIMMONGKOL⁵, CARL LINDENMEYER⁴,
DANIEL C. LONG⁷, JON LOVEDAY¹³, BRYAN MACKINNON^{4,21}, EDWARD J. MANNERY⁵, P.
M. MANTSCH⁴, BRUCE MARGON⁵, TIMOTHY A. MCKAY²², JEFFREY A. MUNN¹⁷,
THOMAS NASH⁴, HEIDI JO NEWBERG⁴, R. C. NICHOL²³, TOM NICINSKI^{4,24}, SADANORI
OKAMURA¹¹, JEREMIAH P. OSTRIKER², RUSSELL OWEN⁵, A. GEORGE PAULS², JOHN
PEOPLES⁴, DONALD PETRAVICK⁴, JEFFREY R. PIER¹⁷, RUTH PORDES⁴, ANGELA
PROSAPIO⁴, RON RECHENMACHER⁴, GORDON T. RICHARDS¹³, MICHAEL W.
RICHMOND²⁵, CLAUDIO H. RIVETTA⁴, CONSTANCE M. ROCKOSI¹³, DALE SANDFORD⁶,
GARY SERGEY⁴, MAKI SEKIGUCHI¹⁴, KAZUHIRO SHIMASAKU¹¹, WALTER A. SIEGMUND⁵,
J. ALLYN SMITH²², CHRIS STOUGHTON⁴, ALEXANDER S. SZALAY⁹, GYULA P. SZOKOLY⁹,
DOUGLAS L. TUCKER⁴, MICHAEL S. VOGLEY², PATRICK WADDELL⁵, SHU-I WANG¹³,
DAVID H. WEINBERG²⁶, NAOKI YASUDA¹², AND DONALD G. YORK¹³

The Astronomical Journal, in press (July 1999)

¹Based on observations obtained with the Sloan Digital Sky Survey, and with the Apache Point Observatory 3.5-meter telescope, which is owned and operated by the Astrophysical Research Consortium

²Princeton University Observatory, Princeton, NJ 08544

³Department of Astronomy and Astrophysics, The Pennsylvania State University, University Park, PA 16802

⁴Fermi National Accelerator Laboratory, P.O. Box 500, Batavia, IL 60510

⁵University of Washington, Department of Astronomy, Box 351580, Seattle, WA 98195

⁶Yerkes Observatory, University of Chicago, 373 W. Geneva St. Williams Bay, WI 53191

⁷Apache Point Observatory, P.O. Box 59, Sunspot, NM 88349-0059

⁸Department of Physics and Astronomy University of Pittsburgh Pittsburgh PA 15260

⁹Department of Physics and Astronomy, The Johns Hopkins University, 3701 San Martin Drive, Baltimore, MD 21218, USA

¹⁰Department of Physics of Complex Systems, Eötvös University, Pázmány Péter sétány 1/A, Budapest, H-1117, Hungary

¹¹Department of Astronomy and Research Center for the Early Universe, School of Science, University of Tokyo, Hongo, Bunkyo, Tokyo, 113-0033 Japan

¹²National Astronomical Observatory, 2-21-1, Osawa, Mitaka, Tokyo 181-8588, Japan

¹³University of Chicago, Astronomy & Astrophysics Center, 5640 S. Ellis Ave., Chicago, IL 60637

¹⁴Institute for Cosmic Ray Research, University of Tokyo, Midori, Tanashi, Tokyo 188-8502, Japan

¹⁵Institute for Advanced Study, Olden Lane, Princeton, NJ 08540

¹⁶Illinois Institute of Technology, 3300 S. Federal Street Chicago, IL 60616

¹⁷U.S. Naval Observatory, Flagstaff Station, P.O. Box 1149, Flagstaff, AZ 86002-1149

¹⁸U.S. Naval Observatory, 3450 Massachusetts Ave., NW, Washington, DC 20392-5420

¹⁹The Observatories of the Carnegie Institution of Washington, 813 Santa Barbara St, Pasadena, CA 91101

²⁰Astronomical Institute, Tohoku University, Aoba, Sendai 980-8578 Japan

²¹Merrill Lynch, 1-1-3 Otemachi, Chiyoda-ku, Tokyo 100, Japan

²²University of Michigan, Department of Physics, 500 East University, Ann Arbor, MI 48109

²³Dept. of Physics, Carnegie Mellon University, 5000 Forbes Ave., Pittsburgh, PA-15232

²⁴Lucent Technologies, 2000 N Naperville Rd, Naperville, IL 60566

²⁵Physics Department, Rochester Institute of Technology, 85 Lomb Memorial Drive, Rochester, NY 14623-5603

²⁶Ohio State University, Dept. of Astronomy, 174 W. 18th Ave., Columbus, OH 43210

ABSTRACT

We present photometric and spectroscopic observations of 15 high-redshift quasars ($z > 3.6$) discovered from $\sim 140 \text{ deg}^2$ of five-color ($u'g'r'i'z'$) imaging data taken by the Sloan Digital Sky Survey (SDSS) during its commissioning phase. The quasars are selected by their distinctive colors in SDSS multicolor space. Four of the quasars have redshifts higher than 4.6 ($z = 4.63, 4.75, 4.90$ and 5.00 , the latter being the highest redshift quasar yet known). In addition, two previously known $z > 4$ objects were recovered from the data. The quasars all have $i^* < 20$ and have luminosities comparable to that of 3C 273. The spectra of the quasars have similar features (strong, broad emission lines and substantial absorption blueward of the Ly α emission line) seen in previously known high-redshift quasars. Although the photometric accuracy and image quality fail to meet the final survey requirements, our success rate for identifying high-redshift quasars (17 quasars from 27 candidates) is much higher than that of previous multicolor surveys. However, the numbers of high-redshift quasars found is in close accord with the number density inferred from previous surveys.

Subject headings: quasars: general; surveys

1. INTRODUCTION

The space density of optically luminous quasars peaks at $z \sim 3$, and declines towards higher redshift (Osmer 1982, Warren, Hewett & Osmer 1994, Schmidt, Schneider & Gunn 1995, Kenefick, Djorgovski & de Carvalho 1995, Hawkins & Véron 1996). The presence of quasars at high redshift provides useful constraints on cosmological models (Efstathiou & Rees 1988, Turner 1991, Eisenstein & Loeb 1995). The evolution of the quasar population at high redshift, and its relation with the evolution of the star forming rate and the intergalactic ionizing background, are important input to our understanding of the formation and early evolution of galaxies (e.g. Boyle & Terlevich 1998, Madau 1998). Meanwhile, the absorption spectra of luminous quasars at high redshift are extremely important in understanding the intergalactic medium (e.g., Rauch 1998).

Since the discovery of the first quasar at $z > 4$ (Warren *et al.* 1987), more than 60 quasars at $z > 4$ have been found (Warren & Hewett 1990, Schneider 1999, Kenefick 1999). However, only 12 quasars at $z > 4.5$ have been identified, of which only one (PC1247+3406, $z = 4.90$, Schneider, Schmidt & Gunn 1991b) has a redshift larger than 4.74. Indeed, Fan (1999) shows that current data are consistent with only one $z > 4.5$ QSO per 50 deg^2 for $i' < 20$.

Most known high-redshift quasars have been selected as outliers in color space from the stellar locus using multicolor broadband photometry (e.g., Warren *et al.* 1987, Kenefick, Djorgovski & de Carvalho 1995, Storrie-Lombardi *et al.* 1996). At $z > 4.5$, the major emission lines and absorption features of quasars are redshifted into the red part of the optical band. Searching for quasars at these redshifts poses three major technical requirements: a red-sensitive detector and filter system, large sky coverage (because of their rarity), and fast, automated software

to do accurate photometry on the resulting large data set.

The Sloan Digital Sky Survey (SDSS; Gunn & Weinberg 1995, SDSS Collaboration 1996, York *et al.* 1999) will use a dedicated 2.5m telescope to obtain CCD images to $\sim 23^m$ in five broad optical bands (u', g', r', i', z' , centered at 3540Å, 4770Å, 6230Å, 7630Å and 9130Å, Fukugita *et al.* 1996) over 10,000 deg^2 of the high Galactic latitude sky centered approximately on the North Galactic Pole. The survey data processing software provides astrometric and photometric calibrations, and finds and measures properties of all detected objects in the data. Spectra of the brightest 10^6 galaxies and 1.5×10^5 quasar candidates will be obtained on the same telescope. The SDSS will select quasar candidates from the much more numerous stars by their distinctive colors, and will generate a large and uniformly-selected sample covering redshifts ranging from $z \sim 0$ to $z > 5$. Because of the large sky coverage and the inclusion of the near-infrared z' band, the SDSS is capable of identifying large numbers of quasars at $z > 4.5$ (Fan 1999).

The SDSS achieved first light in imaging mode in May 1998. By the end of 1998, it had acquired several hundred deg^2 of imaging data in its commissioning phase. Using the ARC 3.5m telescope, we have obtained spectra of a number of high-redshift quasar candidates produced by these data. In this paper, we report the discovery of 15 high-redshift quasars at $z > 3.6$, including four quasars at $z > 4.6$, identified from $\sim 140 \text{ deg}^2$ of SDSS imaging data, 1.4% of the total survey area of the SDSS. In §2, we discuss the photometric observations and data reduction. In §3, we discuss the color selection of high-redshift quasar candidates. The spectroscopic observations of these objects are presented in §4. In §5, we discuss the spectral properties of the quasars. We briefly discuss the success rate and the quasar number counts we find from these data, and compare the number

counts with predictions based on previous results on quasar evolution in §6.

2. PHOTOMETRIC OBSERVATIONS

The SDSS telescope is a dedicated 2.5m altitude-azimuth instrument at Apache Point, New Mexico, with a wide, essentially distortion-free field. It has a modified $f/5.0$ Ritchey-Chretien optical design with a large secondary and two corrector lenses below the primary mirror (Siegmond *et al.* 1999, SDSS Collaboration 1996). Spectroscopy and imaging require separate second correctors. The imaging corrector forms the base structural element for the imaging camera.

The imaging camera (Gunn *et al.* 1998) consists of a mosaic of 30 imaging 2048×2048 SITe CCDs with $24\mu\text{m}$ pixels subtending $0.4''$ on the sky. The CCDs are arranged in six dewars (six columns) containing 5 CCDs each, mounted to the corrector and observing the sky through five broad-band filters. The five filters (u' , g' , r' , i' , and z') cover the entire optical band from the atmospheric cutoff in the blue to the silicon sensitivity cutoff in the red. The u' band, with the bulk of its response shortward of the Balmer discontinuity, is especially important for the selection of low-redshift quasars, while the reddest band, z' , is critical for quasars at $z > 4.5$, where the Ly α emission line enters the i' band. The photometric data are taken in time-delay and integrate (TDI, or “drift-scan”) mode at sidereal rate; a given point on the sky passes through each of the five filters in succession. The total integration time per filter is 54.1 seconds, and the expected survey depth (5σ detection for point sources at $1''$ seeing) is 22.3, 23.3, 23.1, 22.5 and 20.8 in u' , g' , r' , i' , and z' , respectively (but see below). The imaging CCDs saturate at about 14^{m} , so to calibrate these data with existing astrometric catalogs, the camera contains an additional 22 CCDs, each 2048×400 pixels, with neutral density filters that saturate only at 8^{m} (Gunn *et al.* 1998, Pier *et al.* 1999). The data are read from the CCDs, and onto disk and tape using a data acquisition system described in Petravick *et al.* (1994) and Petravick *et al.* (1999).

The SDSS photometric system is based on the AB $_{\nu}$ system:

$$m = -2.5 \log \frac{\int d(\log \nu) f_{\nu} S_{\nu}}{\int d(\log \nu) S_{\nu}} - 48.60, \quad (1)$$

with the zeropoints defined by the spectrophotometric observations of the Oke-Gunn (1983) standard stars (Fukugita *et al.* 1996). The photometric calibration will be carried out with a separate $20''$ photometric telescope equipped with a single-CCD camera and the SDSS filters (Uomoto *et al.* 1999). The photometric telescope will continually observe photomet-

ric standard stars to measure the photometric zeropoint and atmospheric extinction. However, the data used in this paper were taken before the photometric telescope was commissioned; we thus calibrated the data by observing secondary standards in the survey area (cf. Smith *et al.* 1998, Tucker *et al.* 1998) using a (now decommissioned) $24''$ telescope at Apache Point and the US Naval Observatory’s $40''$ telescope. Moreover, the SDSS primary standard star network had not been completely established when these data were taken. Therefore, the absolute photometric calibration is only accurate to 5–10% (although the relative photometry is considerably better). Thus in this paper, we will denote the preliminary SDSS magnitudes we have measured as u^* , g^* , r^* , i^* and z^* , rather than the notation u' , g' , r' , i' , and z' that will be used for the final SDSS photometric system (and is used in this paper to refer to the SDSS filters themselves).

The SDSS data used in this paper were acquired with the telescope parked on the meridian, at the Celestial Equator. Most of the quasar candidates are from data taken in 19 Sept 1998 (SDSS run 94). This observation covers the Northern strip of the equatorial scan (two interleaved scan *strips* are needed to fill in the gaps between different columns of CCDs and form a filled *stripe* 2.5 degrees wide, see Gunn *et al.* 1998). The scan is 6 hours long along the Celestial Equator. The raw data total roughly 120 Gbyte. The scan covers the RA range of $\sim 22^{\text{h}} - 4^{\text{h}}$, with a total area of $\sim 110 \text{ deg}^2$ at high Galactic latitude ($|b| > 40^{\circ}$). The night was photometric, with seeing varying from $1.2''$ to $2.0''$. Because of low-level astigmatism in the 2.5m telescope optics during the early commissioning period, the width of the Point Spread Function (PSF) is also a function of the position of the star on the focal plane. This is an important term in the error budget of the PSF photometry. In addition, one quasar candidate was taken from data obtained on 21 Sept 1998 (SDSS run 109), which covered the Southern strip of the equatorial scan from RA = 2^{h} to 4^{h} , with a total area of $\sim 30 \text{ deg}^2$. The seeing in this scan varied from $1.1''$ to $1.4''$.

These data are processed by a series of automated pipelines to carry out astrometric and photometric measurements. The astrometric pipeline (Pier *et al.* 1999) calibrates the positions of stars with reference to the astrometric standards, and establishes an astrometric solution for each of the imaging CCDs, giving accurate relative astrometry between colors. These data are analyzed with a pipeline (Tucker *et al.* 1998) that measures the magnitudes of secondary standard stars, and sets the photometric zeropoint of the imaging camera, while producing a measure of extinction on each night. The photometric pipeline (PHOTO, Lupton *et al.* 1999b) reduces the data from

the imaging camera and produces corrected images and object catalogs. PHOTO carries out the following tasks:

1. determines smoothly varying flat fields, bias vectors, sky values, and PSFs along each scan line;
2. flat fields the data, interpolates over bad columns, and removes cosmic rays;
3. finds objects in each color as statistically significant peaks after smoothing with the PSF;
4. combines the data from five bands for each object;
5. deblends overlapped objects as described below;
6. measures the position, counts, size and shape of each detected object, and
7. classifies objects as being extended or consistent with point sources, based on fitting simple models.

The final step is to write out calibrated object catalogs using information passed from astrometric and photometric calibrations. Flags indicating image processing problems (such as the presence of saturated pixels, problems with the deblender, and the fact that a cosmic ray has been removed), are also recorded in the output catalogs.

PHOTO measures the PSF magnitude of each source by fitting a PSF model of a double Gaussian. We will use this PSF magnitude throughout the paper. For objects that are undetected in a given band, the PSF fit is constrained to the canonical center of the object in that color, after offsetting according to the astrometric solution. This allows an unbiased measure of the flux of a source even in the case when it is too faint to center up on it. Even though such a measurement is quite noisy, it is very important in distinguishing between red stars and high-redshift quasars (§4).

Overlapping objects are deblended into their constituent parts (“children”) consistently in all five bands. Peaks are found in the image of a given object in each of the five bands, and the union of all the peaks is used to define the children into which the object will be deblended. For each pixel, the deblender assigns weights to each child based on the ansatz that astronomical objects possess a center of symmetry. However, the final deblended children have no such requirement on their symmetry. The output of the deblender is an image of each child in each filter, which are then passed to the object measuring code. Details of the algorithm are given by Lupton (1999).

The final object catalog of Run 94 includes a total of about 2 million objects. The limiting magnitudes are roughly 22.3, 22.6, 22.7, 22.4 and 20.5 in u^* , g^* , r^* , i^* , and z^* , respectively, as determined from the cutoff in the observed number-magnitude relation. This is somewhat brighter than the survey design due to the poor image quality of this run, and the poor reflectivity of the primary mirror (which has since been realuminized). As mentioned above, the absolute photometric calibration is accurate to ~ 0.1 mag, while the relative photometric errors are better than 0.05 mag at $u^* < 20.7$, $g^* < 21.3$, $r^* < 20.8$, $i^* < 20.1$, and $z^* < 18.5$, respectively. The error in the absolute photometric calibration has little effect on the separation of quasars and stars in color space, as it shifts the colors and magnitudes of all objects uniformly.

3. QUASAR SELECTION

Figure 1 presents the color-color diagrams of one column (one-sixth of the total) of the run 94 data for stellar sources at $i^* < 20$. A source is plotted in each panel only if it is detected in all three of the relevant bands. Objects flagged as saturated in any band, lying on the bleed trail of a saturated star, or overlapping the edge of the image boundary have been rejected. However, deblended objects are included in this diagram; their distribution is no broader than that of isolated objects. The group of sources at $g^* - r^* \sim 1.5$ and $r^* - i^* \sim 0.7$ are mostly compact galaxies at $i^* \sim 20$ (i.e., they appear not to be point-like on the images); the star-galaxy classifier was not fine-tuned at faint magnitudes when these data were processed. Note the narrowness of the distributions of all the diagrams. We also plot the median tracks of quasar colors as a function of redshift from the simulation of Fan (1999), and indicate the approximate locations of low-redshift ($z < 2.5$) quasars, hot white dwarfs (WD) and A stars from Fan (1999).

Quasars are well-separated from the stellar locus at most redshifts in the SDSS photometric system, and can be selected by their distinct colors. At $z < 2.0$, quasar optical colors are dominated by the power-law continuum, and the $u^* - g^*$ color of quasars remains smaller than 0.5, considerably bluer than normal stars seen at high latitudes. Ly α emission enters the u' band at $z \sim 2.0$, making the $u^* - g^*$ color even bluer. When Ly α emission moves from u' to g' at $z \sim 2.5$, the $u^* - g^*$ color gets redder. For $z > 2.5$, the absorption systems, first the Ly α forest, then the Lyman Limit Systems (LLSs), enter the u' band. They absorb a substantial fraction of the continuum radiation in u' band, and the $u^* - g^*$ color reddens quickly with redshift. At $z \sim 2.8$, quasars have very similar colors to A stars in the SDSS system.

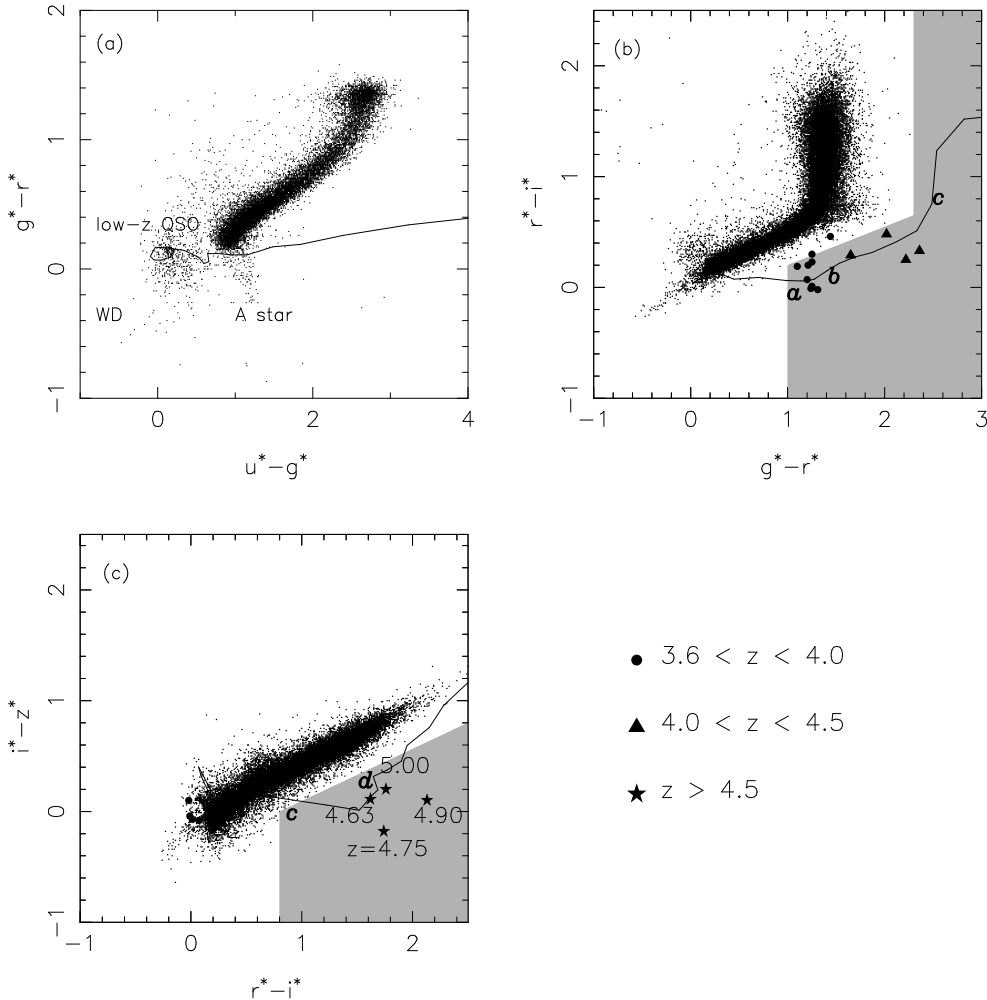


FIG. 1.— Color-color diagrams of stellar objects in 20 deg^2 of SDSS imaging data in Run 94 at $i^* < 20$. The shaded areas on the $g^* - r^*$ vs. $r^* - i^*$ and the $r^* - i^*$ vs. $i^* - z^*$ diagrams represent the selection criteria used to select *gri* and *riz* quasar candidates. The solid line is the median track of simulated quasar colors as a function of redshift (adapted from Fan 1999). The letters a, b, c, and d indicate the positions on the locus of median color quasars at $z = 3.6, 4.0, 4.6$, and 5.0 , respectively. Colors of the 17 confirmed SDSS quasars at $z > 3.65$ are also plotted on the diagrams.

For $z > 3.6$, most quasars are undetectable in u' due to the presence of LLSs, which are optically thick to the continuum radiation from the quasar. Meanwhile, the absorption systems begin to dominate in the g' band, and $\text{Ly}\alpha$ emission moves to the r' band. The $g^* - r^*$ color becomes increasingly red towards higher redshift, while the $r^* - i^*$ color remains relatively small. Quasars at $z > 3.6$ are well-separated from the stellar locus in the $g^* - r^*$ vs. $r^* - i^*$ diagram. At $z > 4.6$, quasars are well-separated from the stellar locus in the $r^* - i^*$ vs. $i^* - z^*$ diagram as the absorption features move into the r' band. The first quasar at $z > 4$ (Warren *et al.* 1987), as well as the highest redshift quasar previously known (Schneider, Schmidt & Gunn 1991b), were discovered using similar methods. Recently, a similar technique has been used to search for high-redshift galaxies, resulting in the discovery of large scale clustering of Lyman

break galaxies at $z > 3$ (Steidel *et al.* 1998) and the first discoveries of galaxies at $z > 5$ (Spinrad *et al.* 1998, Weymann *et al.* 1998).

In the SDSS spectroscopic quasar survey, quasar candidates will be selected by the target selection pipeline (cf. Newberg & Yanny 1997). At the time of writing, this pipeline has not been fine-tuned. Furthermore, the SDSS multi-fiber spectrograph has not yet been commissioned. We therefore have carried out spectroscopic observations of only a small number of objects. We have applied simple color cuts to select only quasars with colors consistent with having $z > 3.6$.

We carry out two separate cuts:

1. *gri* candidates: Quasar candidates with colors consistent with $z > 3.6$, selected principally from their position on the $g^* - r^*$ vs. $r^* - i^*$ diagram. The full selection criteria are:

- (a) $i^* < 20$
- (b) $u^* - g^* > 2.0$ or $u^* > 22.3$
- (c) $g^* - r^* > 1.0$
- (d) $r^* - i^* < 0.2 + 0.42(g^* - r^* - 1.0)$ or $g^* - r^* > 2.3$
- (e) $i^* - z^* < 0.25$

(2)

The region satisfied by criteria (c) and (d) is plotted as the shaded area in Figure 1(b). Criterion (b) selects objects for which most of the flux in u' is absorbed at $z > 3.6$. Criterion (e) provides the additional constraint that the continuum be relatively flat in the red part of the spectrum: this is typical for quasars with power law continua; red stars and compact red galaxies tend to have a much redder $i^* - z^*$.

2. *riz* candidates: Quasar candidates with colors consistent with $z > 4.6$, selected principally from their position on the $r^* - i^*$ vs. $i^* - z^*$ diagram. The full selection criteria are:

- (a) $i^* < 20.2$
- (b) $u^* > 22.3$
- (c) $g^* > 22.6$
- (d) $r^* - i^* > 0.8$
- (e) $i^* - z^* < 0.47(r^* - i^* - 0.8)$

(3)

Quasars at $z > 4.6$ have most of the flux absorbed in the u' and g' bands; such objects are selected with criteria (b) and (c). Criteria (c) and (d) are illustrated in Figure 1(c) as the shaded region. Needless to say, most of the *riz* candidates are undetected in g , and therefore do not show up in Figure 1(b).

We visually inspected the image data in all five filters for all the candidates, paying special attention to those that were deblended from overlapping objects. We deleted from the candidate list obvious problematic cases, such as objects that are close to a saturated star or big galaxy. The final candidate list includes 35 candidates; 25 are *gri* candidates at $i^* < 20$, and 10 are *riz* candidates at $i^* < 20.2$. Eight candidates are deblended from nearby neighbors. Two of the candidates, SDSSp J015339.61-001104.9 and SDSSp J010619.25+004823.4 (see Table 1; for naming convention, see §4), are the previously known quasars BRI0151-0025 ($z = 4.2$) and BRI0103+0032 ($z = 4.43$), found in a multicolor survey (Storrie-Lombardi *et al.* 1996). These two objects are the only quasars with $z > 3.6$ in the area covered by Run 94 found in the NED database²⁷. We matched the candidate list against the FIRST (Becker, White, & Helfand 1995) radio continuum catalog (which covers this area of sky); only one of them has a radio counterpart at 20 cm at the 1mJy level, namely SDSSp J015339.61-001104.9, which is an unresolved source

of 4.75 mJy. We have similarly cross-correlated the list against the ROSAT full-sky pixel images; none of these objects were detected, implying a typical upper limit of 2×10^{-13} erg cm⁻² s⁻¹ in the 0.1-2.4 keV band (W. Voges, private communication).

4. SPECTROSCOPIC OBSERVATIONS

Spectra of 24 high-redshift quasar candidates from Run 94, and one from Run 109, were obtained with the ARC 3.5m telescope in the Apache Point Observatory, using the Double Imaging Spectrograph (DIS) during a number of nights in November and December of 1998. One of the 24 objects observed (SDSSp J025518.58+004847.6) does not satisfy the color selection criteria (eq. 2) with improved photometric calibration, and although we do present its spectrum below, we do not include it in the statistical analysis in §6.

The DIS is a double spectrograph with a transition wavelength of 5350 Å between the blue and red side. The observations were taken with the low resolution gratings, with a dispersion of 6.2 Å pixel⁻¹ in the blue side and 7.1 Å pixel⁻¹ in the red side, and a resolution of roughly 2 pixels. The central wavelengths are 4400 Å and 7700 Å for the blue and red sides, respectively. The final spectrum covers the wavelength range of 4000 Å to 10,000 Å. The wavelength scale is calibrated with a cubic polynomial fit to lines from an Ar-He-Ne lamp; the typical rms error of the fits is smaller than 0.5 Å. Observations of the F subdwarf standards BD+17° 4708 and HD 19445 (Oke & Gunn 1983) provided flux calibration and allowed removal of the atmospheric absorption bands. However, most of the candidates were not observed under photometric conditions, nor were they observed with the slit oriented perpendicular to the horizon. Exposure times ranged from 1200 seconds for an 18 mag candidate to 7200 seconds for the faintest candidates ($i^* \sim 20$).

The data were reduced using both standard software from the IRAF package (by XF), and the procedures described in Schneider, Schmidt, & Gunn (1991a) (by DPS). We place the data on an absolute flux scale (to compensate for the losses due to non-photometric conditions) by forcing the synthetic i^* magnitudes from the spectra to be the same as the photometric measurements. The two independent reductions produce consistent results. Fifteen of the 25 candidates display the characteristics of previously known high-redshift quasars: broad, strong emission lines, and absorption due to the Ly α forest and Lyman Limit systems. The redshifts range from 3.66 to

²⁷The NASA/IPAC Extragalactic Database (NED) is operated by the Jet Propulsion Laboratory, California Institute of Technology, under contract with the National Aeronautics and Space Administration.

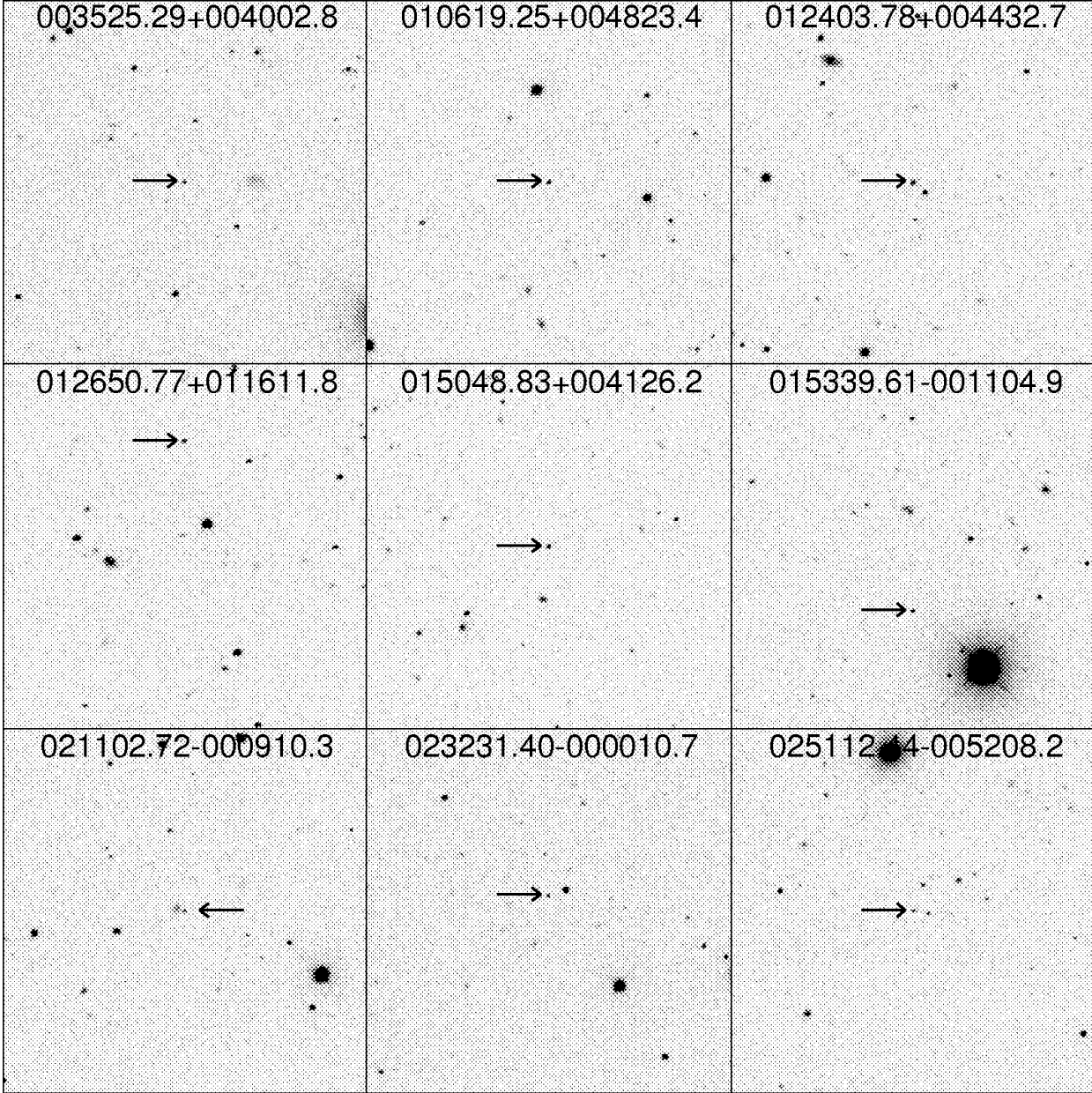


FIG. 2.— Finding charts for the 17 SDSS quasars. The data are $200'' \times 200''$ SDSS images in the i' band (55 sec exposure time). North is up; East is to the left.

5.00; four of the riz candidates are quasars at redshifts 5.00, 4.90, 4.75 and 4.63.

Table 1 gives the position, SDSS photometry and redshift of each confirmed SDSS quasar. We also include in Table 1 the SDSS photometry of the two previously known $z > 4$ quasars in the survey region. The naming convention for the SDSS sources is SDSSp JHHMMSS.SS±DDMMSS.S, where “p”

stands for the preliminary SDSS astrometry (as the astrometric pipeline is still under final commissioning), and the positions are expressed in J2000.0 coordinates. The preliminary SDSS astrometry is accurate to better than $0.2''$ rms in each coordinate. The photometry is actually expressed in asinh magnitudes (Lupton, Gunn, & Szalay 1999), which are identical to ordinary logarithmic magnitudes in the

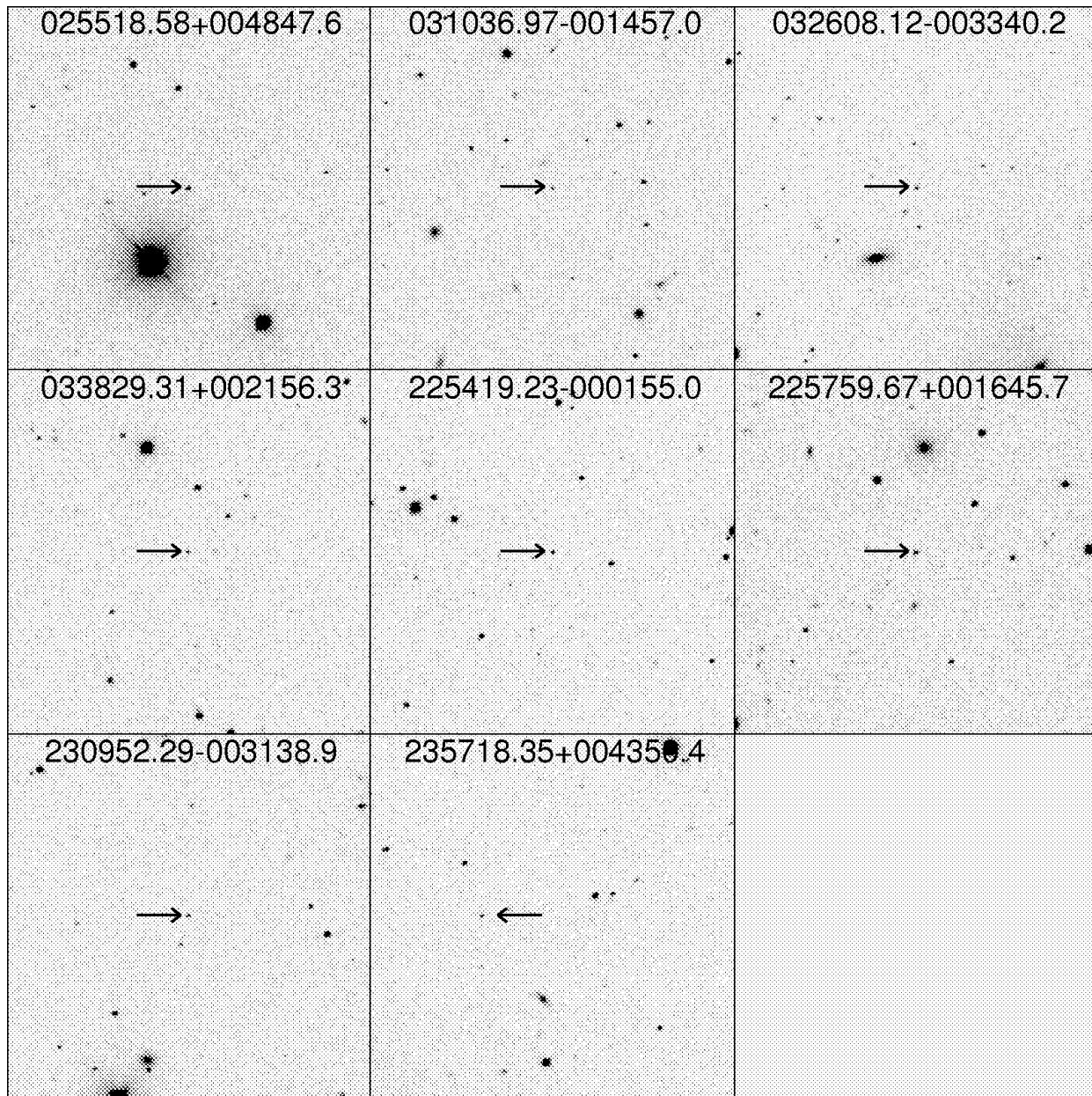


FIG. 2.— Continued

high signal-to-noise ratio regime, but have much better error properties at low signal-to-noise ratio, and indeed allow one to express negative fluxes without simply quoting upper limits. They are described in detail in the Appendix. The errors given are statistical in nature, and do not include systematic errors due to uncertainties in the photometric zeropoint (of order 0.1 mag systematic in each band) and unmodeled variations in the PSF (of order 0.05 mag in each

band).

The $z = 4.90$ quasar (SDSSp J021102.72-000910.3) is deblended from a blue $i^* = 20$ galaxy $5''$ away. This demonstrates that the photometric pipeline is able to deblend close pairs and measure their properties accurately, even for a red point source blended with a blue extended source.

Finding charts of all objects in Table 1 are given in Figure 2. The images are $200'' \times 200''$ SDSS images

TABLE 1
POSITIONS AND PHOTOMETRY OF SDSS HIGH-REDSHIFT QUASARS

SDSS name	redshift	u^*	g^*	r^*	i^*	z^*
SDSSp J003525.29+004002.8	4.75	24.12 ± 0.45	23.63 ± 0.34	21.16 ± 0.06	19.42 ± 0.02	19.60 ± 0.09
SDSSp J010619.25+004823.4 ^a	4.43	23.86 ± 0.43	21.11 ± 0.04	19.09 ± 0.01	18.62 ± 0.01	18.37 ± 0.03
SDSSp J012403.78+004432.7	3.81	22.73 ± 0.20	19.18 ± 0.01	17.87 ± 0.01	17.89 ± 0.01	17.79 ± 0.02
SDSSp J012650.77+011611.8	3.66	22.76 ± 0.28	20.44 ± 0.02	19.20 ± 0.01	19.22 ± 0.02	19.25 ± 0.08
SDSSp J015048.83+004126.2	3.67	23.27 ± 0.29	19.49 ± 0.01	18.39 ± 0.01	18.20 ± 0.01	18.14 ± 0.02
SDSSp J015339.61-001104.9 ^b	4.20	24.01 ± 0.43	21.14 ± 0.04	18.92 ± 0.01	18.67 ± 0.01	18.61 ± 0.04
SDSSp J021102.72-000910.3	4.90	24.04 ± 0.43	24.80 ± 0.54	22.04 ± 0.11	19.93 ± 0.04	19.81 ± 0.13
SDSSp J023231.40-000010.7	3.81	24.87 ± 0.36	21.03 ± 0.03	19.82 ± 0.02	19.62 ± 0.03	19.78 ± 0.12
SDSSp J025112.44-005208.2	3.78	24.81 ± 0.45	20.67 ± 0.02	19.42 ± 0.01	19.41 ± 0.02	19.48 ± 0.10
SDSSp J025518.58+004847.6 ^c	3.97	23.92 ± 0.44	20.53 ± 0.03	19.09 ± 0.01	18.63 ± 0.01	18.65 ± 0.04
SDSSp J031036.97-001457.0	4.63	24.16 ± 0.34	23.41 ± 0.20	21.51 ± 0.06	19.89 ± 0.02	19.77 ± 0.07
SDSSp J032608.12-003340.2	4.16	23.25 ± 0.33	21.14 ± 0.04	19.50 ± 0.02	19.20 ± 0.02	19.07 ± 0.07
SDSSp J033829.31+002156.3	5.00	24.27 ± 0.44	25.03 ± 0.51	21.70 ± 0.09	19.96 ± 0.03	19.74 ± 0.12
SDSSp J225419.23-000155.0	3.68	23.31 ± 0.38	20.80 ± 0.04	19.55 ± 0.02	19.33 ± 0.02	19.27 ± 0.10
SDSSp J225759.67+001645.7	3.75	22.91 ± 0.31	20.11 ± 0.02	18.92 ± 0.01	18.84 ± 0.02	18.92 ± 0.07
SDSSp J230952.29-003138.9	3.95	24.06 ± 0.54	20.95 ± 0.04	19.70 ± 0.02	19.41 ± 0.03	19.42 ± 0.10
SDSSp J235718.35+004350.4	4.34	24.11 ± 0.53	22.43 ± 0.14	20.08 ± 0.03	19.75 ± 0.04	19.58 ± 0.09

Asinh magnitudes (Lupton, Gunn & Szalay 1999; see the Appendix) are quoted; errors are statistical only.

^aThis is the previously known quasar BRI0103+0032 (Storrie-Lombardi *et al.* 1996).

^bThis is the previously known quasar BRI0151-0025 (Storrie-Lombardi *et al.* 1996).

^cThis object is not part of the uniformly selected sample; it falls just outside the color criteria listed in the text.

in the i' band.

Of the ten objects not observed, eight are gri candidates, and two are riz candidates.

Of the ten candidates whose spectroscopy shows them not to be high-redshift quasars, five are late type stars. They are all faint riz candidates, scattered into the selected region due to large photometric errors (especially in z^* , see §6). The low signal-to-noise ratio of the spectra of the remaining five candidates does not allow a definitive classification, but their spectral features are consistent with that of compact galaxies at $z \sim 0.4$ with a very flat continuum for $\lambda_{rest} > 4000 \text{ \AA}$. The broad-band colors inferred from the spectra of these non-quasars are consistent with the SDSS measurements. Some of them may be compact “E+A” galaxies (Dressler & Gunn 1982, Zabludoff *et al.* 1996). At $z \sim 0.4$, their broad-band colors resemble those of quasars at $z \sim 4$. The prominent Balmer jumps in “E+A” galaxies seen through broad-band filters resemble the Lyman break in quasars, while their flat continua from the “A” component in the red resemble the power-law continua of quasars. They are interesting objects in their own right, and will be discussed in a separate paper (cf., Fan *et al.* 1998).

In summary, we have obtained spectra or identi-

fications of 17 of the 25 gri candidates from Run 94. Among them, 2 are previously known quasars, 10 are new SDSS quasars, and 5 are unidentified with spectra consistent with those of compact galaxies. Eight of the 10 riz candidates from Run 94 are identified; 3 are new SDSS quasars at $z = 4.75, 4.90$ and 5.00 , and 5 are late-type stars. Two additional new SDSS quasars are also identified. SDSSp J025518.58+004847.6 ($z=3.97$) was selected from Run 94, but does not meet the color selection criteria (Eq. 2); SDSSp J030136.97-001457.0 ($z=4.63$) was selected from Run 109.

5. SPECTRA OF NEW SDSS QUASARS

Figure 3 gives the low resolution spectra of the 15 new SDSS quasars. Tables 2 and 3 summarize the spectral properties of these quasars.

Table 2 gives the emission line properties. Central wavelengths and rest frame equivalent widths of five major emission lines, OVI λ 1034, Ly α +NV λ 1216+1240, OI+SiII λ 1306, SiIV+OIV] λ 1402, and CIV λ 1549, are measured by Gaussian fitting. In particular, the Ly α +NV blend is fitted to two Gaussians in all but one case. The wavelength given in Table 2 refers to that of the Ly α component, while the equivalent width is the sum

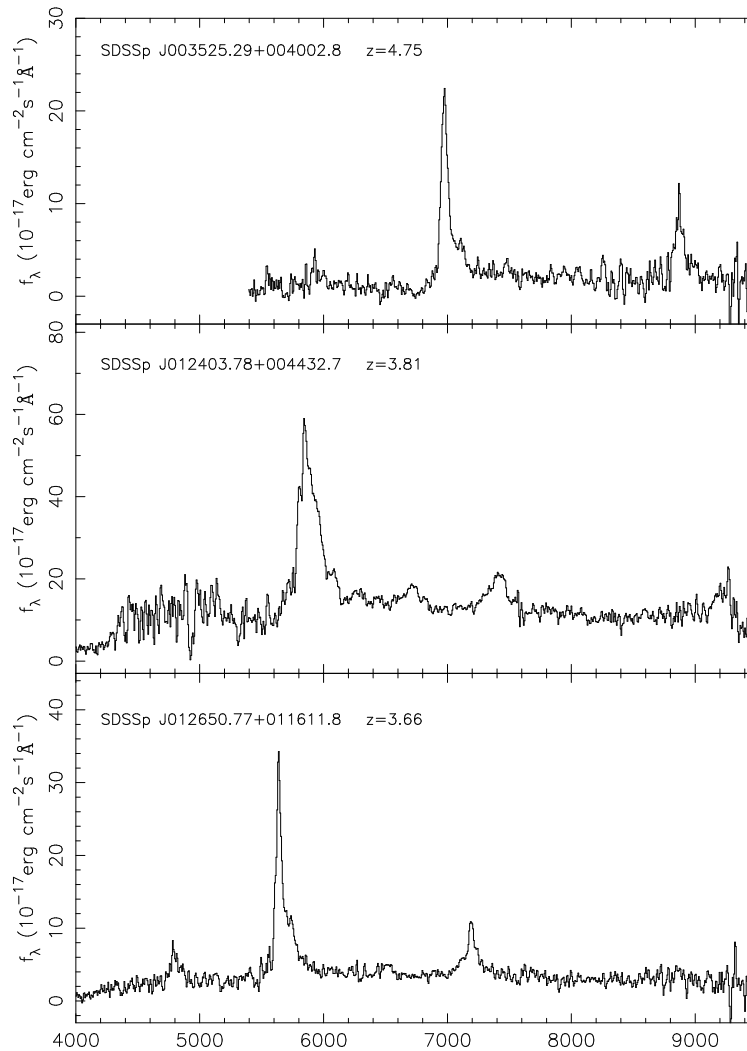


FIG. 3.— ARC 3.5m/DIS spectra of 15 new SDSS quasars. The spectral resolution is about 12 \AA in the blue and 14 \AA in the red. Each pixel represents 12.4 \AA .

of the two. The emission line properties for these quasars are very similar to those of other quasars at $z \gtrsim 4$ (Schneider, Schmidt & Gunn 1989, Schneider, Schmidt & Gunn 1991a, Kenefick, Djorgovski & de Carvalho 1995, Storrie-Lombardi *et al.* 1996). The properties of the four quasars at $z > 4.6$ show no obvious difference from those at lower redshifts (see also Schneider, Schmidt & Gunn 1991b).

The emission line redshift (Table 3) is calculated by taking the weighted mean of the redshift from [OI+SiII, SiIV+OIV] and CIV lines, when they are detected; Ly α is not used because of the strong absorption on its blue side. For all but two cases, at least two of the three lines are detected. Two quasars (SDSSp J021102.72–000910.3 and SDSSp J230952.29–003138.9) have only CIV detected, and we use its redshift here. The uncertainty in redshift determination is dominated by discrepancies of the redshifts of different lines. The statistical error from a single line measurement is typically much smaller.

The redshift uncertainty quoted in Table 3 is the scatter of the measurements from different lines. If the scatter is smaller than 0.01 (or in the cases when only CIV is detected), we adopt a lower limit of 0.01.

Table 3 also gives AB₁₄₅₀, the AB magnitude of the quasar continuum at 1450 \AA (rest frame) and M_B of each quasar. They are corrected for Galactic extinction using the reddening map of Schlegel, Finkbeiner & Davis (1998). We use a cosmology of $q_0 = 0.5$, $h = 0.5$, and a power law index of -0.5 for the quasar continuum when calculating M_B . The absolute magnitudes are comparable to that of 3C 273, which is $M_B = -27$ in this cosmology.

Although the quality of our spectra is not high, precluding an accurate measurement of the flux decrement due to the Ly α forest, more than 70% of the continuum radiation blueward of Ly α emission line is absorbed by the forest for our highest-redshift quasars. This is quite consistent with what has been seen with previously known quasars at similar red-

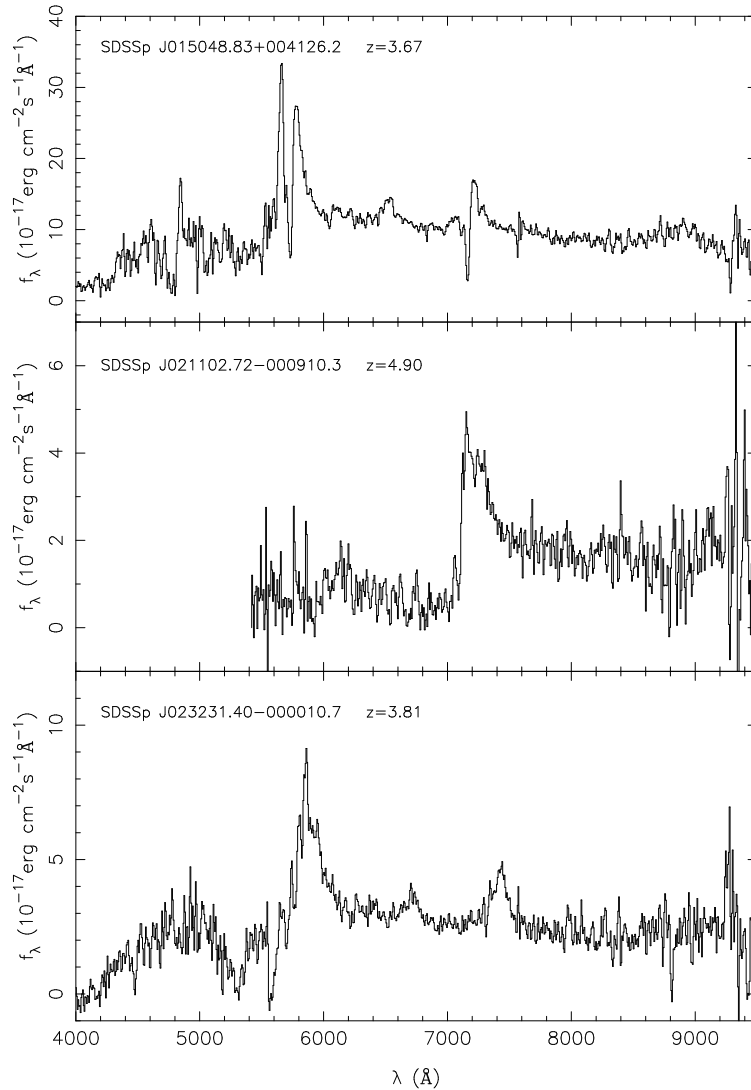


FIG. 3.— Continued

shifts.

Strong Lyman Limit Systems (LLSs) are visible in all quasars that have sufficient signal-to-noise ratio in that part of the spectra. Their corresponding redshifts are listed in Table 3. For the four quasars at $z > 4.6$, the spectra near the Lyman Limit are too noisy to decide where the absorption occurs. In addition, there are several damped Ly α absorption line candidates (also listed in Table 3); one quasar shows evidence of a Broad Absorption Line (BAL) system.

5.1. Notes on Individual Objects

SDSSp J003525.29+004002.8 ($z = 4.75$). This quasar shows very strong Ly α and CIV lines. It has a detectable OI+SiII line, but the SiIV+OIV] line is undetected, the only such case among the 15 quasars. **SDSSp J015048.83+004126.2** ($z = 3.67$). This is a mini-BAL quasar (e.g., Barlow, Hamann, & Sargent 1997, Churchill *et al.* 1999), with strong self-absorption in all detected lines. The CIV trough has a FWHM of $\sim 4000 \text{ km s}^{-1}$. The LLS at $z_{abs} = 3.71$

is probably associated with the BAL.

SDSSp J023231.40-000010.7 ($z = 3.81$). The strong Ly α absorption feature at 5610 \AA is at the same redshift as the LLS in this quasar.

SDSSp J032608.12-003340.2 ($z = 4.16$). The spectrum reveals two features that could be $\tau < 1$ LLSs at $z_{abs} = 4.15$ and 4.00 . There is a large optical depth LLS at $z_{abs} = 3.67$.

SDSSp J033829.31+002156.3 ($z = 5.00$). This is the quasar with the highest known redshift to date. The Ly α , SiIV+OIV] and CIV lines are clearly detected, but an accurate redshift determination is not straightforward. The Ly α emission line yields a redshift of 5.08 , but its blue wing is strongly affected by absorption. The other two lines detected, SiIV+OIV] and CIV, give a consistent redshift of 5.00 . However, the SiIV+OIV] line is quite weak, while the red side of the CIV line is strongly affected by the strong atmospheric absorption at 9300 \AA . The redshift determination is quite uncertain. We have adopted a redshift of 5.00 ± 0.04 for this object.

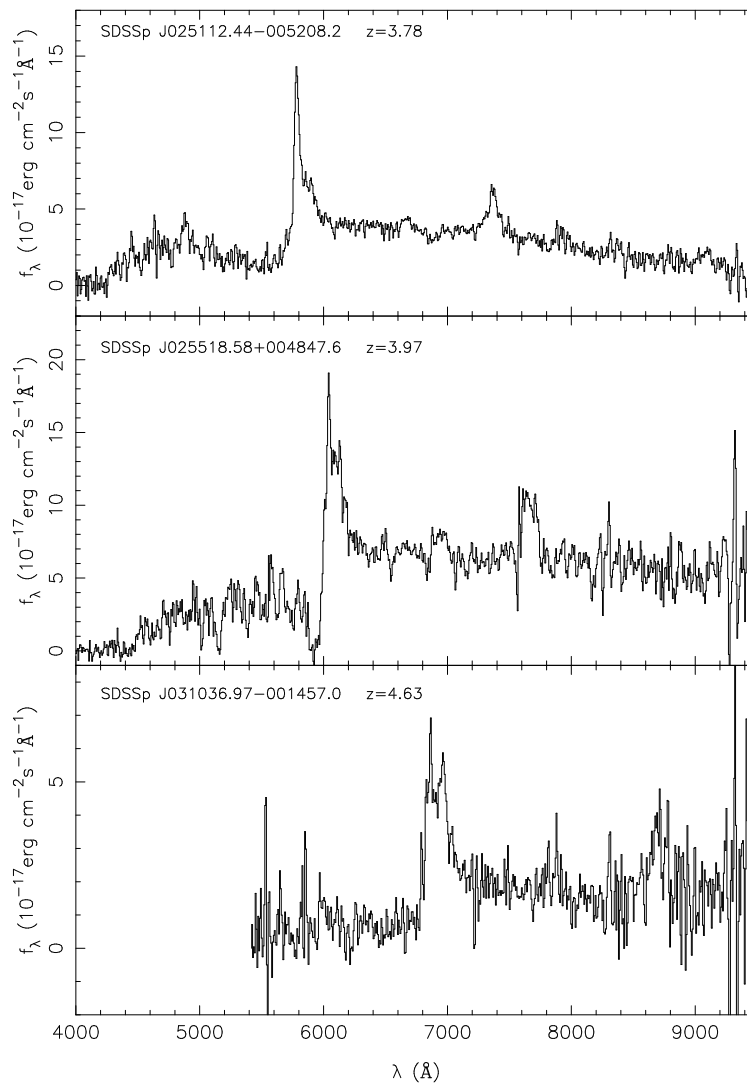


FIG. 3.— Continued

6. DISCUSSION

The success rate of the quasar search from these SDSS commissioning data is substantially higher than that of previous multicolor surveys at similar magnitude and redshift range (e.g. Kennefick, Djorgovski & de Carvalho 1995, Hall *et al.* 1996). Although the current sample is not complete, among the 25 uniformly selected candidates in Run 94 (including the 2 previously known high-redshift quasars) that have been identified, 15 are quasars at $z > 3.6$, a success rate of 60%, while previous surveys have had success rates less than 20%. In particular, among the 17 *gri* candidates that are identified, 12 are quasars at $z > 3.6$, a success rate of 70%. This is due to two reasons: (1) the high photometric accuracy of the SDSS data; and (2) the fact that we have been very conservative in our candidate selection (§3). We expect that as we extend our candidate search to fainter flux levels and nearer to the stellar locus, our success rate will decline.

The success rate of *riz* candidates appears much lower (3 quasars out of 8 candidates in Run 94, or 38%). The random photometric error in the z' band is 0.15 mag at $z^* \sim 19.8$ for Run 94. For quasars at $z \sim 5$, where we must rely on the z' measurements, a large contamination from red stars is expected.

Although the SDSS can detect quasars at z up to 7 in the z' band, selection of quasars at $z > 5.5$ (if they exist) may prove quite difficult. Figure 1(c) shows that the quasar locus approaches the locus of very late type stars; this happens for redshifts $z > 5$. At even higher redshifts, quasars become undetectable in the r' band, and additional information in the near IR may be required to distinguish quasars from very red late type stars (such as L-type stars, Kirkpatrick *et al.* 1999).

The survey we have presented here does not result in a complete sample for three reasons. First, the photometric calibration of these data is preliminary and has larger errors than what will be achieved by the SDSS after the commissioning period. This

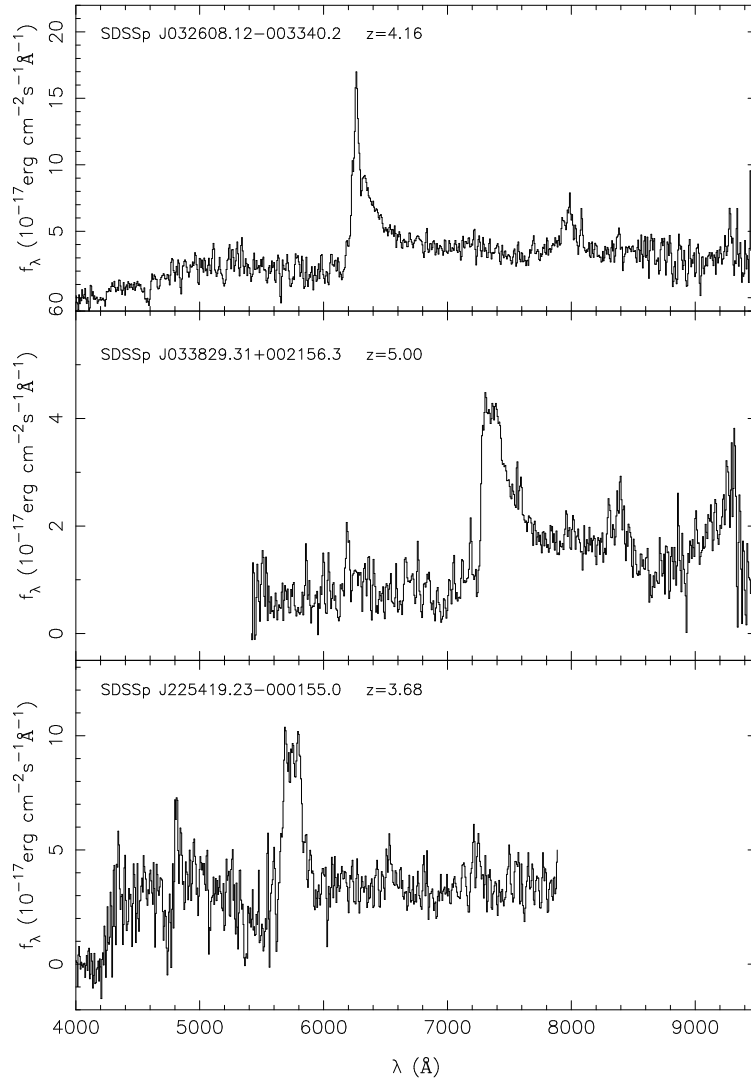


FIG. 3.— Continued

will affect the selection of our sample at some level, although already our photometric accuracy is superior to that of most previous multicolor searches for high-redshift quasars. Second, the color cuts applied on the data, although objective, are largely arbitrary. They may miss a considerable fraction of high-redshift quasars, although we have seen that the quasars we have found follow the model quasar locus quite closely. Third, we have not yet finished observing all our candidates.

The current data do not allow us to calculate the selection function reliably, so we do not intend to calculate the quasar number density or luminosity function at high-redshift from these quasars at this time. However, as a consistency check, we compare the number of quasars observed to date with the predicted number counts from Fan (1999) in Table 4. Fan (1999) predicts the quasar number counts in SDSS bands based on the quasar luminosity function of Pei (1995) for $z < 4$ and Schmidt, Schneider & Gunn (1995) for $z > 4$. The quasar number counts are based on those

identified from Run 94 (110 deg²). Since we have not observed all the high-redshift quasar candidates, nor do we address the problem of completeness, the observed numbers in Table 4 are only lower limits. Within the errors from small number statistics, the predicted numbers and the numbers observed are consistent. Table 4 shows that although previous surveys have been less efficient than the present work, there is no indication that they missed a large fraction of high-redshift quasars.

Even though the data in this study have not yet achieved the SDSS survey standards in imaging quality and in photometric calibrations, the high quality CCD data and powerful survey software enable efficient selection of high-redshift quasars. The data described in this paper cover only $\sim 1\%$ of the SDSS survey area. The largest samples that have been used in determining the evolution of the quasar luminosity function at $z > 4$ consist of only ~ 10 quasars (Schmidt, Schneider & Gunn 1995, Kennefick, Djorgovski & de Carvalho 1995). In the entire SDSS sur-

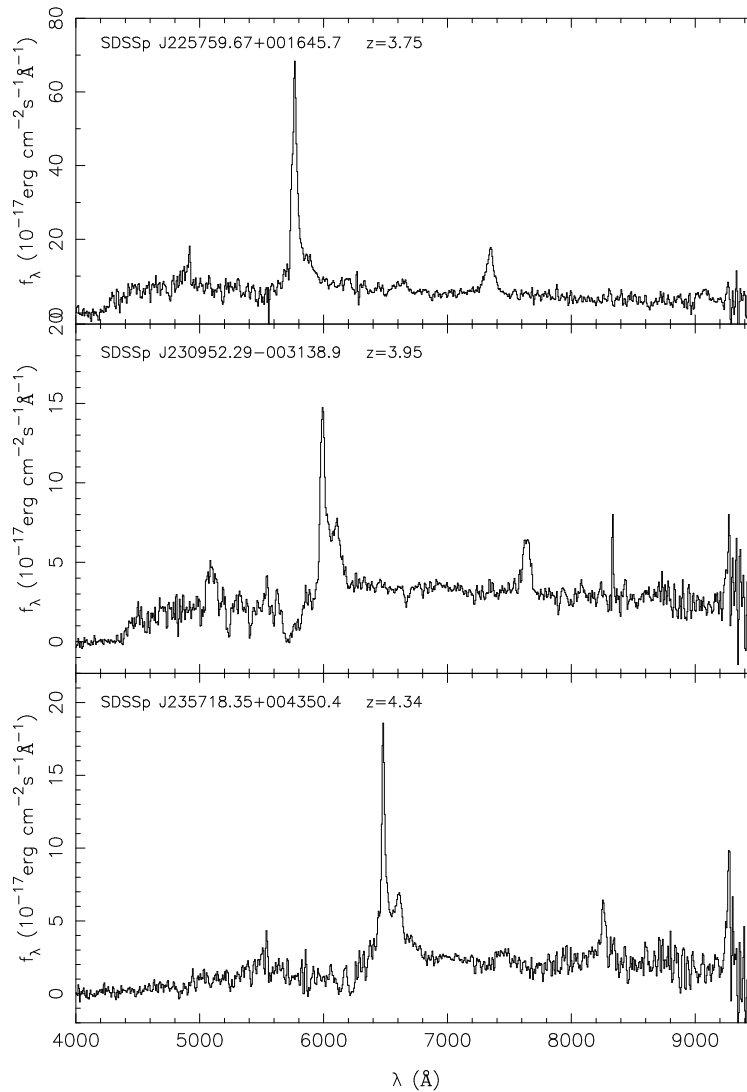


FIG. 3.— Continued

vey, we expect to find ~ 600 quasars with $z > 4$ at $i' < 20$, with a significant number of them at $z > 5$. These quasars will be selected uniformly and will cover a large area of the sky. This sample will be invaluable in understanding the large scale distribution and evolution of high-redshift quasars, as well as providing bright quasars at high redshift for detailed studies of quasar absorption systems.

The Sloan Digital Sky Survey (SDSS) is a joint project of the University of Chicago, Fermilab, the Institute for Advanced Study, the Japan Participation Group, The Johns Hopkins University, the Max-Planck-Institute for Astronomy, Princeton University, the United States Naval Observatory, and the University of Washington. Apache Point Observatory, site of the SDSS, is operated by the Astrophysical Research Consortium. Funding for the project has been provided by the Alfred P. Sloan Foundation, the SDSS member institutions, the National Aeronautics and Space Administration, the National Science Foundation, the U.S. Department of Energy,

and the Ministry of Education of Japan. XF and MAS acknowledge additional support from Research Corporation, NSF grant AST96-16901, the Princeton University Research Board, and an Advisory Council Scholarship. DPS acknowledges the support of NSF grant AST95-09919. We thank Wolfgang Voges for useful comments on the manuscript. We also thank the usual expert assistance of Bruce Gillespie, Karen Gloria, Camron Hastings, Tia Hoyes, and Russet McMillan.

APPENDIX: THE DEFINITION OF ASINH MAGNITUDES

Lupton *et al.* (1999a) describe the rationale for a refinement of the usual logarithmic magnitude scale, to better handle the low signal-to-noise ratio regime, and the possibility of zero fluxes. The asinh magnitude for an object of observed flux f is defined as

$$\mu(f) = \mu(0) - a \sinh^{-1} \left(\frac{f}{2b'} \right) \quad (4)$$

TABLE 2
EMISSION LINE PROPERTIES OF SDSS HIGH-REDSHIFT QUASARS

quasar	OVI 1034	Ly α 1216+1240	OI+SiII 1306	SiIV+OIV] 1402	CIV 1549
SDSSp J003525.29+004002.8	5955 \pm 5	7002 \pm 1	7509 \pm 10		8899 \pm 4
	15.4 \pm 4.2	82.4 \pm 5.7	16.6 \pm 2.3		66.4 \pm 5.4
SDSSp J012403.78+004432.7		5879 \pm 1	6317 \pm 7	6744 \pm 5	7434 \pm 3
		74.2 \pm 1.6	5.2 \pm 0.6	10.6 \pm 0.7	24.8 \pm 0.9
SDSSp J012650.77+011611.8	4832 \pm 2	5661 \pm 1		6535 \pm 12	7221 \pm 4
	38.5 \pm 1.3	76.0 \pm 7.3		18.6 \pm 2.3	50.1 \pm 1.9
SDSSp J015048.83+004126.2		5707 \pm 2		6559 \pm 4	7226 \pm 4
		47.9 \pm 2.6		7.9 \pm 0.7	24.0 \pm 0.9
SDSSp J021102.72-000910.3		7187 \pm 3			9138 \pm 24
		60.9 \pm 9.7			39.7 \pm 6.9
SDSSp J023231.40-000010.7		5880 \pm 4		6740 \pm 9	7451 \pm 5
		48.6 \pm 5.7		10.1 \pm 1.5	23.7 \pm 1.5
SDSSp J025112.44-005208.2	4916 \pm 4	5812 \pm 1		6697 \pm 15	7396 \pm 4
	17.5 \pm 1.5	75.1 \pm 5.1		7.1 \pm 1.7	19.2 \pm 1.4
SDSSp J025518.58+004847.6		6069 \pm 2	6520 \pm 12	6968 \pm 12	7671 \pm 5
		31.8 \pm 2.6	2.3 \pm 1.0	8.4 \pm 1.3	26.4 \pm 1.8
SDSSp J031036.97-001457.0		6886 \pm 3		7892 \pm 19	8727 \pm 10
		56.9 \pm 6.7		19.2 \pm 4.6	47.7 \pm 5.8
SDSSp J032608.12-003340.2		6292 \pm 1		6740 \pm 9	7451 \pm 5
		58.8 \pm 4.6		6.4 \pm 1.9	22.0 \pm 2.2
SDSSp J033829.31+002156.3		7386 \pm 8		8419 \pm 12	9299 \pm 12
		71.5 \pm 14.5		20.3 \pm 3.4	13.9 \pm 3.0
SDSSp J225419.23-000155.0		5782 \pm 8		6561 \pm 9	7265 \pm 7
		87.2 \pm 17.7		8.2 \pm 1.9	12.9 \pm 2.2
SDSSp J225759.67+001645.7	4925 \pm 4	5794 \pm 1		6657 \pm 11	7371 \pm 2
	19.7 \pm 1.6	72.3 \pm 6.8		10.6 \pm 2.1	36.1 \pm 1.9
SDSSp J230952.29-003138.9	5125 \pm 1	6020 \pm 1			7667 \pm 3
	20.1 \pm 0.7	63.8 \pm 2.7			15.5 \pm 0.9
SDSSp J235718.35+004350.4		6510 \pm 1		7486 \pm 9	8286 \pm 2 7
		47.1 \pm 2.4		12.5 \pm 2.1	20.2 \pm 1.5

The two entries in each line are the central wavelength and rest frame equivalent width from the Gaussian fit to the line profile, both measured in Ångstroms.

TABLE 3
CONTINUUM PROPERTIES OF SDSS HIGH-REDSHIFT QUASARS

quasar	redshift	AB ₁₄₅₀	M_B	z_{LLS}	z_{abs}^a
SDSSp J003525.29+004002.8	4.75 ± 0.01	19.95	−26.66		
SDSSp J012403.78+004432.7	3.81 ± 0.02	18.07	−28.19	3.71	3.08
SDSSp J012650.77+011611.8	3.66 ± 0.01	19.58	−26.62	3.57?	
SDSSp J015048.83+004126.2	3.67 ± 0.01	18.35	−27.75	3.71	
SDSSp J021102.72−000910.3	4.90 ± 0.02	20.02	−26.63		
SDSSp J023231.40−000010.7	3.81 ± 0.01	19.72	−26.54	3.61	3.61, 3.37
SDSSp J025112.44−005208.2	3.78 ± 0.01	19.55	−26.70	3.67	
SDSSp J025518.58+004847.6	3.97 ± 0.02	18.66	−27.67	3.94	3.89, 3.26
SDSSp J031036.97−001457.0	4.63 ± 0.01	20.06	−26.78		
SDSSp J032608.12−003340.2	4.16 ± 0.02	19.19	−27.21	4.15	
SDSSp J033829.31+002156.3	5.00 ± 0.04	20.01	−26.56		
SDSSp J225419.23−000155.0	3.68 ± 0.01	19.48	−26.73	3.64	
SDSSp J225759.67+001645.7	3.75 ± 0.01	19.05	−27.19	3.63	
SDSSp J230952.29−003138.9	3.95 ± 0.01	19.50	−26.82	3.82	3.73, 3.32
SDSSp J235718.35+004350.4	4.34 ± 0.01	19.86	−26.61	4.29	4.14, 4.06

Absolute magnitudes assume $H_0 = 50 \text{ km s}^{-1} \text{ Mpc}^{-1}$, and $q_0 = 0.5$.

^aThese are redshifts of damped Ly α lines seen in the spectra.

TABLE 4
NUMBER COUNTS IN 110 DEG²: PREDICTED VS. OBSERVED (LOWER LIMIT FROM RUN 94)

	predicted	observed
$z > 3.6, i' < 19$	3.0	7
$z > 3.6, i' < 20$	18.1	15
$z > 4.0, i' < 19$	1.2	2
$z > 4.0, i' < 20$	6.3	7
$z > 4.5, i' < 20$	1.9	3

TABLE 5
PARAMETERS ASSOCIATED WITH ASINH MAGNITUDES

Filter	b'	m_0	$\mu(0)$
u^*	0.46	23.40	24.24
g^*	0.53	24.22	24.91
r^*	0.60	23.98	24.53
i^*	0.70	23.51	23.89
z^*	0.55	21.83	22.47

The softening parameter b' (in units of DN/second), magnitude zero points m_0 corresponding to a count rate of 1 DN per second for SDSS imaging run 94, and asinh magnitude $\mu(0)$ at zero flux for the preliminary SDSS color system u^* , g^* , r^* , i^* , and z^* . The b' values are fixed for the SDSS, but the $\mu(0)$ values are of course determined for each run separately.

where $a \equiv 2.5/\ln 10 = 1.08574$, $\mu(0)$ is a normalizing magnitude, setting the zero-point of the scale, and b' is a softening parameter. We set b' equal to the sky noise within a PSF, which optimizes the error properties of this modified magnitude. For signal-to-noise ratios greater than 5, these magnitudes are essentially identical to standard logarithmic magnitudes.

We have adopted this magnitude scale for the measurements given in Table 1. For reference, a detection of zero flux has magnitude $\mu(0)$, and a formal error of 0.52 mag in this system, thus a 1- σ detection of flux has an asinh magnitude $\mu(0) - 0.52$. The values of $\mu(0)$ and b are given in Table 5 for each color.

REFERENCES

- Barlow, T.A., Hamann, F., & Sargent, W.L.W. 1997, in *Mass Ejection from AGN*, ASP Conference Series 128, eds N. Arav, I. Shlosman, and R.J. Weymann (PASP:San Francisco), 13
- Becker, R.H., White, R.L., & Helfand, D.J. 1995, ApJ, 450, 559
- Boyle, B.J., & Terlevich, R.J. 1998, MNRAS, 293, 49
- Churchill, C.W., Schneider, D.P., Schmidt, M. & Gunn, J.E. 1999, AJ, in press
- Dressler, A., & Gunn, J.E. 1982, ApJ, 263, 533
- Efstathiou, G. & Rees, M.J. 1988, MNRAS, 230, 5
- Eisenstein, D.J., & Loeb, A. 1995, ApJ, 443, 11
- Fan, X. 1999, AJ, in press, astro-ph/9902063
- Fan, X. *et al.* 1998, BAAS, 30, 1244
- Fukugita, M., Ichikawa, T., Gunn, J.E., Doi, M., Shimasaku, K., & Schneider, D.P. 1996, AJ, 111, 1748
- Gunn, J.E., *et al.* 1998, AJ, 116, 3040
- Gunn, J.E. & Weinberg D.H. 1995, in *Wide Field Spectroscopy and the Distant Universe* ed. S. Maddox & Aragón-Salamanca (World Scientific, Singapore), 3
- Hall, P.B., Osmer, P.S., Green, R.F., Porter, A.C., & Warren, S.H. 1996, ApJ, 462, 614
- Hawkins, M.R.S. & Véron, P. 1996, MNRAS, 281, 348
- Kennefick, J.D. 1999, <http://www-astronomy.mps.ohio-state.edu/~julia/quasars/all.html>
- Kennefick, J.D., Djorgovski, S.G., & de Carvalho, R.R. 1995, AJ, 110, 255
- Kirkpatrick, D., *et al.* 1999, ApJ, submitted
- Lupton, R.H. 1999, in preparation
- Lupton, R.H., Gunn, J.E., & Szalay, A. 1999a, AJ, submitted (astro-ph/9903081)
- Lupton, R.H. *et al.* 1999b, in preparation; see also <http://www.astro.princeton.edu/BBOOK/DATASYS/datasys.html>
- Madau, P. 1998, in *The Birth of Galaxies*, eds. B. Guiderdoni, F. R. Bouchet, T. X. Thuan, & T. T. Van, in press
- Newberg, H.J., & Yanny, B. 1997, ApJS, 113, 89
- Oke, J.B., & Gunn, J.E. 1983, ApJ, 266, 713
- Osmer, P.S. 1982, ApJ, 253, 28
- Pei, Y.C. 1995, ApJ, 438, 623
- Petravick, D., *et al.* 1994, SPIE, 2198, 935
- Petravick, D., *et al.* 1999, in preparation
- Pier, J. *et al.* 1999, in preparation, see also <http://www.astro.princeton.edu/BBOOK/ASTROM/astrom.html>
- Rauch, M. 1998, ARA&A, 36, 267
- Schlegel, D.J, Finkbeiner, D.P., & Davis, M. 1998, ApJ, 500, 525
- Schmidt, M., Schneider D.P., & Gunn, J.E. 1995, AJ, 110, 6
- Schneider, D.P. 1999, in *After the Dark Ages: When Galaxies were Young (the Universe at $2 < z < 5$)*, in press
- Schneider, D.P., Schmidt, M. & Gunn, J.E. 1989, AJ, 89,1951
- Schneider, D.P, Schmidt, M., & Gunn, J.E. 1991a, AJ, 101,2004
- Schneider, D.P, Schmidt, M., & Gunn, J.E. 1991b, AJ, 102, 837
- SDSS Collaboration 1996, "SDSS Black Book", <http://www.astro.princeton.edu/BBOOK/>
- Siegmund, W. *et al.* 1999, in preparation, see also <http://www.astro.princeton.edu/BBOOK/TELESCOP/telescope.html>
- Smith, J.A. *et al.* 1998, BAAS, 30, 1244
- Spinrad, H., Stern, D., Bunker, A., Dey, A., Lanzetta, K., Yahil, A., Pascarelle, S., & Fernández-Soto, A., 1998, AJ, 116, 2617
- Steidel, C.C., Adelberger, K.L., Dickinson, M., Giavalisco, M., Pettini, M., & Kellogg, M.A. 1998, ApJ, 492, 428
- Storrie-Lombardi, L.J., McMahon, R.G., Irwin, M.J., & Hazard, C. 1996, ApJ, 468, 121
- Tucker, D.L. *et al.* 1998, BAAS, 30, 1245
- Turner, E.L. 1991, AJ, 101, 5
- Uomoto, A. *et al.* 1999, in preparation, see also <http://www.astro.princeton.edu/BBOOK/PHOTCAL/photcal.html>

- Warren, S.J., & Hewett, P.C. 1990, Rep. Prog. Phys., 53, 1095
- Warren, S.J., Hewett, P.C., Irwin, M.J., McMahon, R.G.,
Bridgeland, M.T. 1987, Nature, 325, 131
- Warren, S.J., Hewett, P., & Osmer, P.S. 1994, ApJ, 421, 412
- Weymann, R.J., Stern, D., Bunker, A., Spinrad, H., Chaffee,
F.H., Thompson, R.I., & Storrie-Lombardi, L.J. 1998, ApJ,
505, L95
- York, D. *et al.* 1999, in preparation,
see also [http://www.astro.princeton.edu/BBOOK/
INTRO/intro.html](http://www.astro.princeton.edu/BBOOK/INTRO/intro.html)
- Zabludoff, A.I., Zaritsky, D., Lin, H., Tucker, D., Hashimoto,
Y., Shectman, S.A., Oemler, A., & Kirshner, R.P. 1996, ApJ,
466, 104